PCCP

PAPER

View Article Online
View Journal | View Issue

Electronic and structural study of Pt-modified Au vicinal surfaces: a model system for Pt–Au catalysts†

Cite this: *Phys. Chem. Chem. Phys.*, 2014, **16**, 13329

Mauricio J. Prieto,* Emilia A. Carbonio,* Shadi Fatayer, Richard Landers and Abner de Siervo

Received 3rd April 2014,
Accepted 14th May 2014

DOI: 10.1039/c4cp01448k

www.rsc.org/pccp

Two single crystalline surfaces of Au vicinal to the (111) plane were modified with Pt and studied using scanning tunneling microscopy (STM) and X-ray photoemission spectroscopy (XPS) in ultra-high vacuum environment. The vicinal surfaces studied are Au(332) and Au(887) and different Pt coverage (θ_{Pt}) were deposited on each surface. From STM images we determine that Pt deposits on both surfaces as nanoislands with heights ranging from 1 ML to 3 ML depending on θ_{Pt}. On both surfaces the early growth of Pt ad-islands occurs at the lower part of the step edge, with Pt ad-atoms being incorporated into the steps in some cases. XPS results indicate that partial alloying of Pt occurs at the interface at room temperature and at all coverage, as suggested by the negative chemical shift of Pt 4f core line, indicating an upward shift of the d-band center of the alloyed Pt. Also, the existence of a segregated Pt phase especially at higher coverage is detected by XPS. Sample annealing indicates that the temperature rise promotes a further incorporation of Pt atoms into the Au substrate as supported by STM and XPS results. Additionally, the catalytic activity of different PtAu systems reported in the literature for some electrochemical reactions is discussed considering our findings.

1. Introduction

Transition metals (TMs) have been used in the last decades as crucial components in materials with industrial application such as catalysts in heterogeneous or electrocatalysis. Practical applications range from binary or ternary alloys in the form of nanoparticles supported in more inert materials such as TM oxides or high surface area carbon powder,[1–9] to thin films deposited on a variety of surfaces.[10]

Particularly, in the field of fuel cells, Pt has been extensively used among other TMs as one of the active components on binary or even ternary alloys supported on C for oxidation of small organic molecules[7,11–13] with the aim of finding a suitable catalyst with technological applications.

On the other hand, single crystalline surfaces of low Miller index have been used in the last decades to elucidate the most fundamental properties of the catalysts that would allow eventually a rational design of more efficient materials. As a result, it was determined that surface effects have an important role on the mechanism of chemical or electrochemical reactions. For instance, reactions involving the breaking of a chemical bond can be enhanced by the presence of uncoordinated atoms on the surface of the catalyst.[14]

From a fundamental point of view, vicinal or high index surfaces have offered the possibility of studying in a very controlled way the role of these surface defects on the fundamental steps of chemical reactions. A vicinal surface is a single crystalline surface whose surface normal is tilted by a few degrees (vicinal) from the normal of a given basal plane. As a result, the surface consists of terraces having a defined width and crystallographic orientation separated by steps of monoatomic height. Therefore, by properly selecting the direction and the miscut angle, step density and crystallographic orientation of both terrace and step can be tuned.

Two vicinal surfaces of gold were used in the present study, named Au(332) and Au(887). The first surface can be described as Au(S) [5(111) × (110)] and the second as Au(S) [15(111) × (110)]. It has been reported in the literature that the Au(887) surface undergoes a surface reconstruction similar to the (22 × $\sqrt{3}$) reconstruction of the Au(111) face, with discommensuration lines running in the direction perpendicular to the step-edge. As a result, stacking fault lines separating fcc and hcp surface layer stacking emerge on terraces as in the herringbone reconstruction of Au(111).[15,16] These two type of sites open the possibility of creating nanoarrays of foreign

Departamento de Física Aplicada, Instituto de Física Gleb Wataghin, Universidade Estadual de Campinas, 13083-859, Campinas, SP, Brazil. E-mail: prietomauricio@gmail.com, emiliacarbonio@gmail.com

† Electronic supplementary information (ESI) available. See DOI: 10.1039/c4cp01448k

metals due to preferential deposition as it has been demonstrated by Rousset and coworkers.[17–19]

In a general approach, the modification of the properties of the constituents in bimetallic catalysts has been explained through three main effects: ensemble, ligand and geometric.[20–22] The first effect is related with the arrangement of atoms where the reaction that is being catalyzed occurs (atomic ensemble). The second effect derives from the fact that the energies of adsorption of the reactants, products or intermediate species can be modified by changing the electronic structure of the metallic component of the bimetallic system. Finally, the geometric effect is related to the changes in catalytic properties of the catalyst due to modifications on the interatomic distances (lattice strain) due to lattice mismatch between the metallic components.

The Pt–Au system has attracted the attention of the scientific community because of its promising results for reactions such as hydrocarbon conversion,[23] formic acid oxidation[11] and oxygen reduction.[24,25] In model catalysis, the Pt/Au(*hkl*) system also represents the interesting case of study where a very reactive metal (Pt) is diluted in a relatively inert matrix (Au). Moreover, the lattice mismatch between Au and Pt is 4%, sufficient to induce modification on the properties of Pt and Au due to tensile stress.

In this paper we report the results of the electronic and structural properties of two vicinal Au surfaces modified with different amounts of Pt. We show how the crystallographic orientation of the substrate determines the growth mode of Pt and, through photoelectron spectroscopy, how the electronic properties of Pt are modified by the substrate. Finally, we discuss the implications of our findings in the interpretation of experimental electrocatalytic behavior of Pt–Au systems.

2. Experimental

2.1 Equipment

All experiments were carried out in an ultra-high vacuum (UHV) system. The chamber is equipped with LEED optics, an SPECS-Phoibus 150 hemispherical electron analyzer with nine-channeltron detection, an Ar ion gun for sputtering, a water cooled evaporator and a high precision two rotation axis manipulator, allowing sample transfer and heating up to 1200 K by electron bombardment. The setup operates in a base pressure better than 5×10^{-10} mbar regime during evaporation and measurements. The XPS experiments were performed using Mg Kα line and all spectra were collected at 60° from surface normal. Additionally, the sample could be transferred directly to an adjoining chamber equipped with an Aarhus 150 (SPECS) scanning tunneling microscope (STM) operating under UHV, available for STM measurements with a tungsten tip in constant current mode. The operating base pressure during image acquisition was always within the 10^{-11} mbar range and operating conditions (I_{tunnel} and V_{bias}) are described on each figure's caption. WSxM[26] software was used for image processing.

All metallic components were fitted using a Doniach–Šunjić function[27] and a Shirley background. Bulk values of parameters such as lifetime width of Au and Pt 4f lines and asymmetry factor were used since, as demonstrated by Hörnström[28] and Shevchik[29] *et al.* these parameters remain unaffected upon dilution in bulk Pt–Au alloys. The resulting fittings of all samples can be seen in the ESI.† A value of 71.09 eV for Pt $4f_{7/2}$ core line was taken as reference for bulk Pt.[30]

2.2 Sample preparation

Au single crystals were obtained from Mateck GmbH as 10 mm discs oriented in the (332) and (887) directions with surface roughness lower than 0.03 micron and orientation accuracy better than 0.1 degree. Au surfaces were meticulously cleaned prior to Pt deposition using consecutive cycles of sputtering and annealing. Sputtering was performed using Ar^+ ions at 1–1.5 keV. Initially, long sputtering times were needed to remove surface contamination, but once the surface was clean 10–15 min of sputtering at 1 keV were enough to achieve a reproducible surface. Annealing of the crystals at 798 K were necessary to regenerate the previously damaged surface with annealing times ranging from 10 to 30 min. XPS measurements were performed between cycles to follow oxygen and carbon 1s photoelectron lines in order to ensure the effectiveness of the cleaning methodology. Once a clean state of the surface was achieved, STM and LEED measurements were performed and Pt was deposited by e-beam evaporation from an exhaustively degassed tip of a Pt (99.997%) wire at constant rate which was previously calibrated. Deposition time was varied in order to obtain different coverage and all deposits were investigated using XPS and STM at room temperature.

3. Results and discussion

3.1 Clean vicinal Au surfaces

Before the study of the morphological and electronic properties of the modified surfaces, it is mandatory to determine the quality of Au substrates used as templates for Pt growth. STM images obtained for clean Au(332) and Au(887) surfaces are shown in Fig. 1a and c. For both surfaces, the periodic nature of the steps is evident form STM images, proven by the parallel lines equally spaced running in a given direction. Analyzing the high resolutions STM images in Fig. 1b and d the characteristic packing of the (111) plane on the terraces is clearly visible. The periodicity of steps for each vicinal surface reflects the number of atoms constituting the terrace and the differences can be seen on the topographic profiles presented in Fig. 1e and f. Terrace width for both vicinal surfaces were calculated from a collection of STM images (not shown) and the values obtained are 13.6 ± 0.6 and 41 ± 1 Å in good agreement with values reported in the literature for both surfaces.[15,18,31,32] Au–Au interatomic distance was determined as being 2.8 ± 0.1 Å from topographic profile in Fig. 1g. It is worth mentioning that both surfaces gave similar results for $d_{Au–Au}$ within the experimental error. Additionally, for the (332) face the existence of kinks is clearly seen from the high resolution image. On the other hand, in the case of the (887) face, kink formation was not detected.

Additionally, on Au(887) the existence of a reconstruction is clear from the bright lines running perpendicular to step

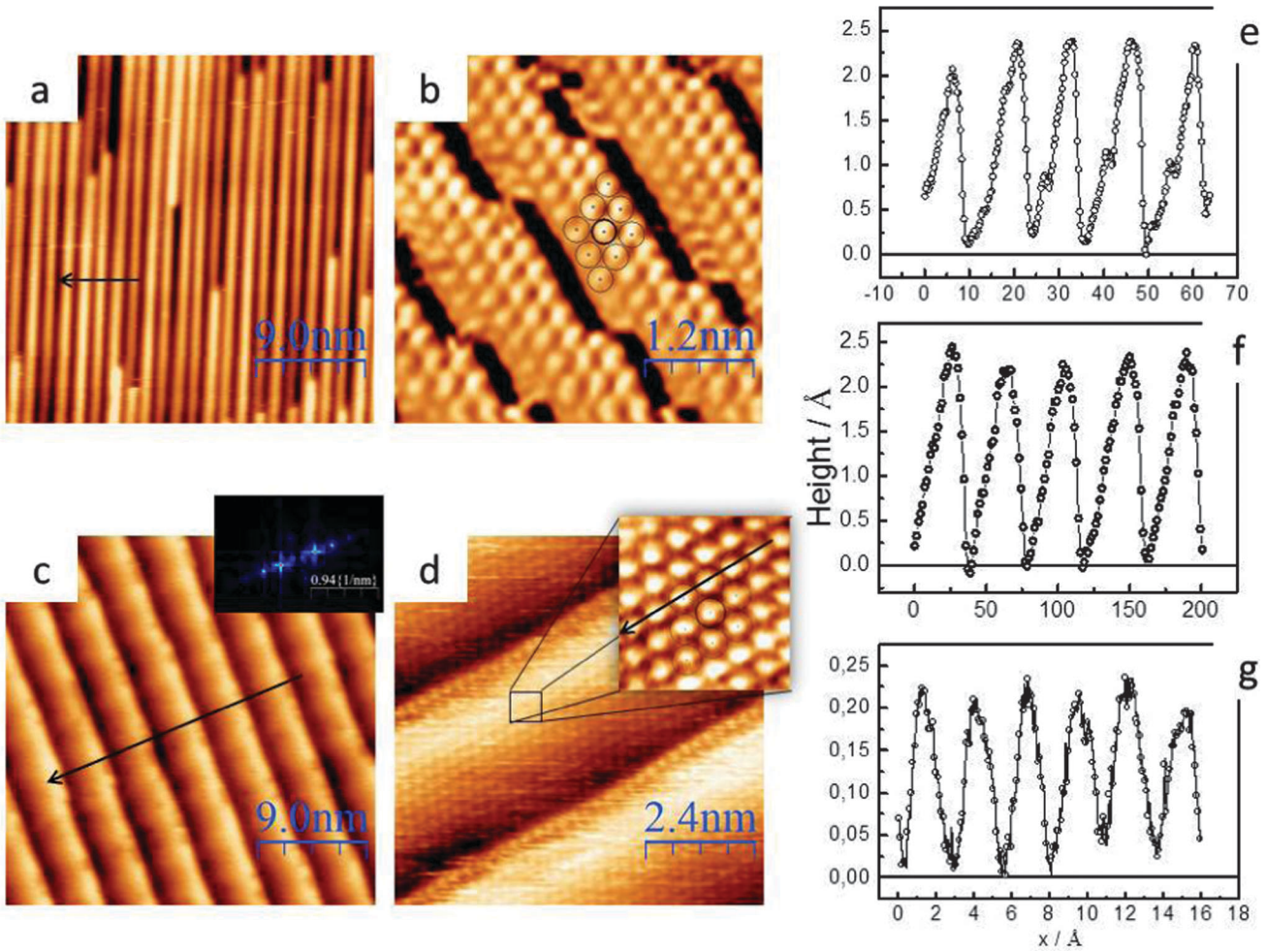

Fig. 1 STM images obtained for clean Au(332) (a, b) and Au(887) (c, d). Inset in (c) corresponds to FFT 2D pattern of STM image. Topographic profiles showing periodic nature of terraces are displayed in (e) and (f) for Au(332) and Au(887), respectively. Atomic profile from inset in (d) is shown in (g). Tunneling conditions are: (a, b) I_{tunnel} = 0.11 and 0.30 nA, V_{bias} = 1.2 and 1.7 V; (c, d) I_{tunnel} = 0.160 and 1.730 nA, V_{bias} = 1.2 and 0.42 V.

edges (Fig. 1c). This reconstruction has already been described in the literature by other authors as being similar to the $(22 \times \sqrt{3})$ reported for Au(111), consisting of discommensurate lines that run perpendicular to the step edge, with the creation of alternating fcc/hcp stacking sites along the terrace with a periodicity of 71 Å.[15,18,33] In the case of Au(332) such reconstruction is not detected, probably due to the small size of the terrace; *i.e.*, the formation of alternating fcc–hcp sites along the 5 atom wide terrace would introduce an additional strain which is energetically less favorable than the unreconstructed surface.

Fig. 2 shows LEED patterns obtained for both clean surfaces after repeated cycles of sputtering and annealing. Both LEED patterns reflect the 3-fold symmetry associated with the (111) face. In addition, spot splitting due to the superstructure formed by the existence of steps is observed for both surfaces. In the particular case of Au(887) surface, the nature of spot splitting in LEED pattern has been explained by Repain *et al.*,[34] and the existence of multiple diffraction spots in two perpendicular directions (see inset Fig. 2b) has been taken as a proof of long range order of steps and the surface reconstruction. From LEED patterns the $W_{terrace}/d_{Au-Au}$ ratio of 4.6 and 13.6 were obtained from diffraction spots for Au(332) and (887), in very good agreement with the ratio calculated from theoretical values (4.6 and 13.3, respectively) using the hard sphere model of the surface and a lattice constant of 4.08 Å. The addition and subtraction of an atomic row were also considered for the calculation of the theoretical values of the ratio and the results are very different from the experimentally obtained from LEED. These results, together with the morphology observed by STM, indicate the correct assignment of surface orientation in both cases.

3.2 Morphologic and electronic characterization of Pt/Au(332) and Pt/Au(887)

Fig. 3 shows STM images of Pt-modified surfaces for three different coverage of Pt on each Au(*hkl*) vicinal surface. As can be seen from the STM images the new Pt phase is not equally structured on both vicinal surfaces studied. For instance, in the case of Au(887), a regular array of Pt nanostructures is formed, as described in the literature for various transition metals deposited on the same surface.[17,19,31,34–36]

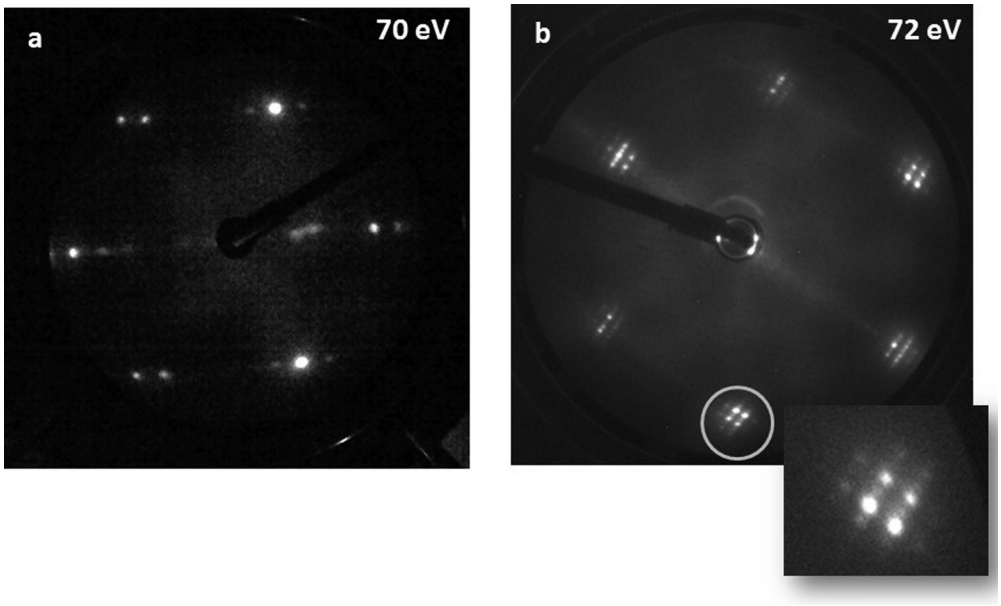

Fig. 2 LEED patterns for clean Au(332) (a) and Au(887) (b). Inset: magnification of the region within the grey circle in (b) showing the spot splitting on Au(887).

In the specific case of the Pt/Au(887) system, nucleation and growth begin at the lower part of the step edge and the growth proceeds all over the terrace as θ_{Pt} increases, filling up the fcc site, as also observed by Nahas *et al.*[17] In the case of the Au(332), we believe the same site preference for nucleation applies, as both surfaces belong to the same family of planes. However, due to the lack of surface reconstruction on the underlying Au substrate and consequently to the absence of any kind of preferential site along the narrow (111) terrace, the growth of Pt nanoislands occurs with an elongated shape in the direction parallel to the step edge, suggesting the lack of site preference on the terrace as in Au(887). These results suggest that, at room temperature, the energy barrier for Pt ad-atom diffusion on the terrace should be overcome on both surfaces, allowing atoms initially arriving at the terrace to diffuse towards the nearest step edge, where nuclei begin to grow. Moreover, since a step acts as a potential barrier for ad-atom diffusion across the step edge line, there is a preferential orientation for Pt island to grow on the parallel direction of step edge, in the same way we also observed for Co growth on Au(332).[37]

As stated by Antczak and Ehrlich,[38] the presence of steps on a surface modifies the surface potential landscape in different ways depending on the nature of the surface and the foreign atom and these modifications may well not be just short ranged. The authors reviewed the results published over the last decades regarding the surface diffusion (self and hetero diffusion) on stepped surfaces as well as in basal planes of several transition metals. Among all the systems reviewed, Au(331) (self-diffusion) and Pt/Au(110) (hetero-diffusion) systems were considered. The results shown by the authors indicate that surface diffusion can be classified into two types of diffusion depending on the direction of motion: one parallel to the step or so called in-channel and one across the steps called cross-channel. Their conclusion is that in-channel diffusion, *i.e.* diffusion along a terrace is energetically more favorable than cross-diffusion over the step edge. It is clear from data presented by the authors that the magnitude of the activation energy for diffusion in both scenarios strongly depends on the ad-atom on the surface and the mechanism of diffusion (hoping *vs.* exchange or even multiple events).

For the specific case of Pt ad-atoms on Au, there is a lack of experimental data in the literature regarding the study of diffusion phenomena. However, results obtained by Kim *et al.*[39] using the so called *action-derived molecular dynamics* procedure, indicate that Pt diffusion on Au(110) surface occurs following the hoping mechanism and in the direction parallel to the step edge (in-channel). These results agree with our findings regarding the anisotropic growth previously mentioned in the case of Au(332).

On the other hand, it has been already reported by Liu *et al.*[40] that on the reconstructed $(22 \times \sqrt{3})$ Au(111) the binding energy for an ad-atom on the fcc site is larger than on the hcp site. Additionally, these authors reported relatively high activation energy for surface diffusion from an fcc-like to an hcp-like site ($\sim$0.5 eV). In view of the fact that in the Au(887) surface these two sites coexist along the terrace, the accumulation of Pt on the fcc site observed experimentally (see Fig. 3d–f) matches the picture predicted by their theory. However, it is important to mention at this point that, as can be observed in the inset of Fig. 3f, when coverage is drastically increased to 1.48 ML, some structures associated with Pt deposition become appreciable on hcp sites. In this case, we observed that the height of islands on fcc sites contiguous to the hcp ones accommodating these structures are equivalent to 3 ML, suggesting that Pt deposition on fcc site may no longer be stable compared to the deposition on hcp site, beyond this coverage limit. Nevertheless, surface concentration of hcp-Pt seems to be low, even at the highest coverage studied.

Fig. 4 shows two topographic profiles traced in the direction parallel to the step edge for Pt/Au(887) with θ_{Pt} = 0.29 and 0.59.

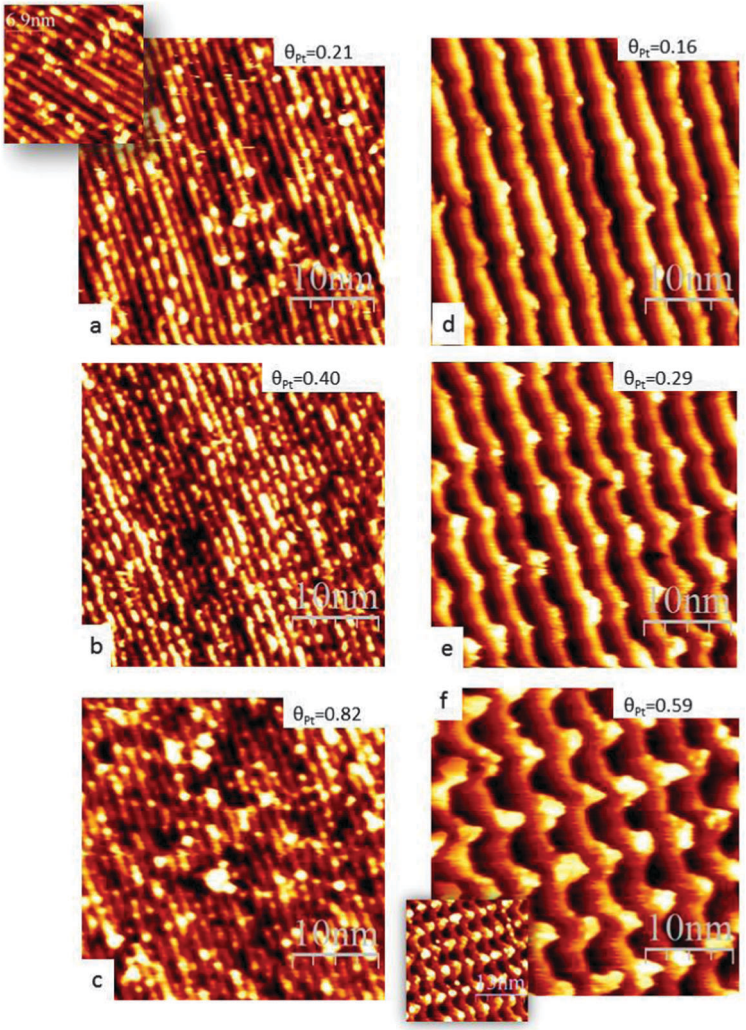

Fig. 3 STM images of Pt deposits on Au vicinal surfaces. (a–c) Pt/Au(332) and (d–f) Pt/Au(887). Pt coverage is indicated on each image. Tunneling conditions: (a) V_{bias} = 1.7 V; I_t = 0.55 nA; (b) V_{bias} = 1.25 V; I_t = 0.36 nA; (c) V_{bias} = 1.5 V; I_t = 0.56 nA; (d) V_{bias} = 1.24 V; I_t = 0.45 nA; (e) V_{bias} = 1.32 V; I_t = 0.32 nA and (f) V_{bias} = 1.25 V; I_t = 0.36 nA. Insets in (a) and (f) correspond to Pt/Au(332) with θ_{Pt} = 0.18 and Pt/Au(887) with θ_{Pt} = 1.48, respectively.

Considering the theoretical value of 2.26 Å for a monoatomic height of a Pt island,[41] we determine that there is a monolayer to bilayer transition in the growth mode of Pt nanoislands on the fcc sites of Au(887) as coverage increases. Also, the FFT of STM image shown in Fig. 3f evidences the long-range nanopatterning of the surface due to preferential nucleation at fcc sites. The periodicity of the nanostructures were calculated from STM image as being 69.93 ± 0.05 Å, in good agreement with the periodicity suggested of the fcc–fcc stacking lines on the clean reconstructed Au surface. A close inspection of a different sample with θ_{Pt} = 1.48 (inset in Fig. 3f) reveals that the bilayer growth regime is extended to higher Pt coverage with a topographic profiles similar to that shown in Fig. 4b. Manual counting of the number of islands having different heights from topographic profiles reveals that, for the sample with θ_{Pt} = 0.29, all the islands analysed have a monoatomic height. As platinum coverage increases to 0.59 ML, only 5% of Pt nanoislands preserve the monoatomic height, while 92% of the islands are bilayers. When the θ_{Pt} = 1.48 ML sample is analysed we see that the number of bilayered islands decreases to 72% of the total count, while the amount of islands having a 3 ML height increases from 3% (for the θ_{Pt} = 0.59 ML sample) to 16%.

On the other hand, the quantification of islands height in Pt/Au(332) in the same way as for Pt/Au(887) is not possible due to the difficulty in determining the boundaries of the islands on the topographic profiles from the STM images shown in Fig. 3a–c. However, based on the fact that the maximum heights measured for all Pt/Au(332) samples are comparable to those measured for Pt/Au(887), we assume that in the case of Pt/Au(332) nanoislands have also ML and BL heights and, since the crystallographic orientation on the terrace is the same on both vicinal gold substrates, that the same ML to BL transition is observed as coverage increases, even though the terrace width is considerably narrower.

The Pt–Au system has been studied by some authors using STM in the form Pt/Au(*hkl*)[42] or Au/Pt(*hkl*)[22] for basal planes of both platinum and gold. Also, Nahas *et al.*[17] studied the Pt/Au(887) system using variable temperature STM with deposition temperatures up to 300 K. For instance, Pedersen *et al.*[42] observed, by using

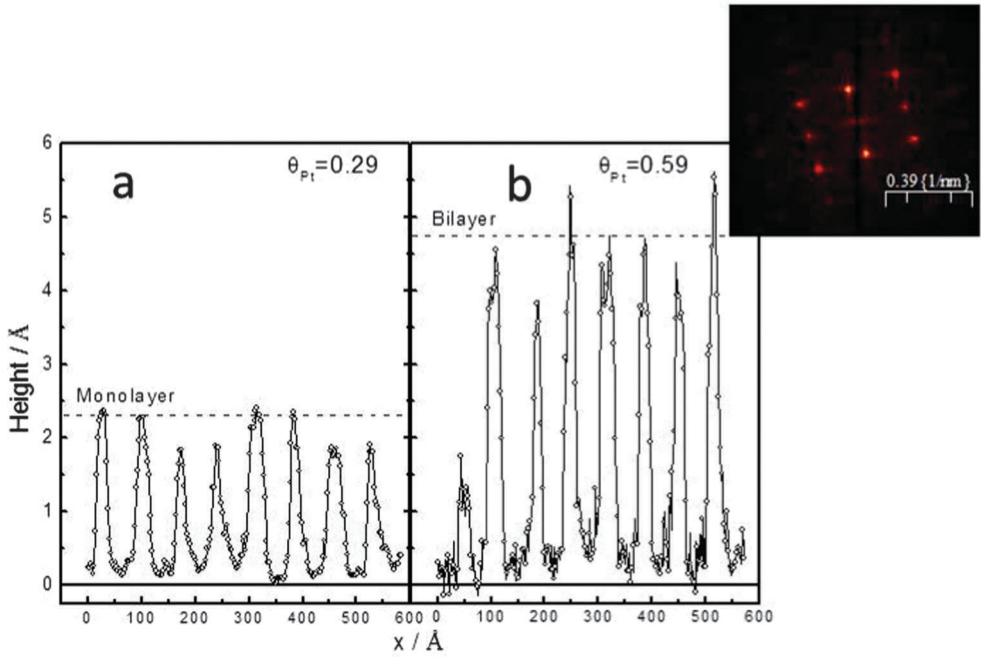

Fig. 4 Topographic profiles sketched from STM images of Fig. 3e and f for Pt/Au(887). Pt coverage as indicated. Inset in (b) corresponds to FFT of image shown in Fig. 3e, showing the periodicity of Pt nanoislands.

chemical contrast, the formation of a substitutional Pt–Au alloy with variable composition, where Pt atoms tend to be capped by Au atoms throughout an exchange process. On the other hand, Nahas *et al.*[17] found in the case of Pt/Au(111) that nanoislands are composed mainly of Pt based on a 15 pm difference in height lower than the reference of Au(111) step height, suggesting that the results observed by Pedersen may be a result of contamination by CO. Moreover, the authors mention in their paper[17] that the exchange process of Au atoms by incoming Pt ad-atoms is a thermally activated process and it should be kinetically hindered at temperatures lower than the growth temperature used by them (room temperature). Still, both papers report the preferential deposition of Pt atoms on the elbows of the herringbone reconstructed Au(111) surface.

From the theoretical point of view, Gohda and Groß[43] studied the Pt/Au(111) using first principle calculations and came to the conclusion that alloy formation with a 2 ML thickness have lower enthalpy of formation than those having 1 ML height. However, the formation of a Pt–Au alloyed layer should be an endothermic process according to their calculations, although under any experimental given conditions, the thermodynamic state of surface alloys may be far from equilibrium, at a metastable state. In this sense, our results indicate that on both vicinal surfaces the nanoisland's height is coverage dependent, with the bi-layers being favored at middle range coverage. Moreover, when coverage is further increased even the formation of nanoislands of three atomic layers is observed by STM. Nevertheless, since atomic resolution was not achieved for both Pt/Au(*hkl*) surfaces, it is not possible to say, solely from our STM results, what is the composition of the nanoislands, *i.e.* pure Pt or Pt–Au alloy, an issue that will be addressed in the next section with the aid of photoelectron spectroscopy.

In order to determine the electronic properties of the Pt/Au(*hkl*) interfaces, X-ray photoemission spectra were collected for all samples. The XPS spectra obtained for the as prepared samples showing the Au 4f and Pt $4f_{7/2}$ regions are presented in Fig. 5. By applying a fitting procedure of photoelectron spectra we determined the existence of at least two contributions to the 4f core line of Pt. Also, changes in the intensity ratio of these two contributions are clear from spectra as platinum coverage increases, regardless of the crystallographic orientation of the underlying Au surface. The BE values of the different components of the Pt $4f_{7/2}$ line obtained from the fitting are listed in Table 1 (for fitted spectra see ESI†). BE values for Au 4f photoemission lines are also reported in Table 1, although for all Pt coverage studied, the BE of the lines remain unchanged upon deposition within the resolution achieved under the current experimental conditions.

As can be seen from data in Table 1, two main components were detected in Pt $4f_{7/2}$ core line. The components are separated as $BE_{Pt/Au(hkl)} < BE_{bulkPt}$ (component A) and $BE_{Pt/Au(hkl)} > BE_{bulkPt}$ (component B). It has been reported[28,29,44] that for Pt–Au bulk alloys a shift of the same magnitude and direction (BE < bulk value) on 4f core lines is observed upon dilution, both for Pt and Au 4f lines, with the magnitude of the chemical shift being dependent on the composition of the alloy. The comparison of our results with those observed for bulk Pt–Au alloys suggests that a fraction of Pt atoms, especially at the low coverage limit, might be incorporated into the topmost atomic layer of Au crystal, and that the extent of this incorporation seem to be independent on terrace width, since similar chemical shifts were observed on Au(332) and Au(887).

In this context, the model proposed by Pedersen *et al.*[42] for the Pt/Au(111) model system is extremely important to explain

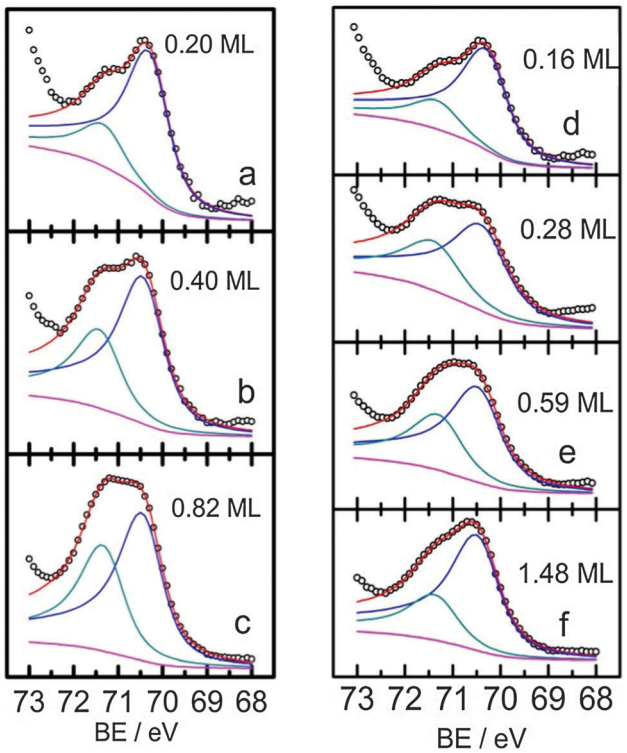

Fig. 5 Photoemission spectra and fitting results of Pt $4f_{7/2}$ core line for all Pt/Au(*hkl*) samples. (a–c) Pt/Au(332) and (d–f) Pt/Au(887). Pt coverage as indicated.

the existence of component A in photoelectron spectra of Fig. 5 (see Table 1). The authors were able to image using an STM operating at low temperature the formation of what they called a substitutional alloy, especially at very low coverage ($\theta_{Pt} < 0.1$ ML). The idea of incorporation of Pt atoms into the topmost layer of Au atoms was considered due to a difference of about 0.35 Å in the topographic height in the vicinity of bright spots in high resolution STM images. It was also found that, although alloy formation dot not exhibit any type of ordering, it takes place preferentially on the upper part of the step edge or near the stacking fault domain boundaries of the herringbone reconstruction.

Consequently, the Au atoms displaced from their original position nucleate into 2D islands on the surface, offering additional sites for Pt deposition as platinum coverage rises. Thus, 2D islands formed are bimetallic, with their composition being dependent on the Pt equivalent loading. Since the crystallographic orientation of the terraces on both surfaces is the same used by the authors in ref. 42 we believe that the same alloying mechanism is responsible for the existence and dislocation of component A in our XPS spectra. Also, similarly to the case of the Au(111), we believe, based on our observation and on the models for surface diffusion mentioned earlier, that at the low coverage limit the exchange process of Au by Pt atoms might occur at the step edge rather than on terrace (see *e.g.* Fig. 3d).

On the other hand, the component B on the Pt $4f_{7/2}$ line that appears at BE > Pt_{bulk} shifted by as much as 0.3 eV (ΔE_B) can be related to Pt that is segregated without being alloyed with Au (see Table 1). It is well known from the literature that, for nanoparticles, BE values for photoemission core lines shift to higher BE as nanoparticle's size decreases. For instance, Keister *et al.*[45] studied the Pt/SiO_2 system varying θ_{Pt} using synchrotron radiation. The authors observed chemical shifts of up to 1 eV for Pt coverage as low as 0.3 ML, the latter being comparable with the coverage studied in the present paper over Au(*hkl*). In the case of the Pt/SiO_2 sample, these shifts were explained by the fact that during the photoemission experiments the photoelectron emitting center becomes instantaneously charged and the resulting electrostatic potential depends on the size of the Pt cluster/island, thus making BE of photoemission core 4f lines size dependent.

Combining STM and XPS results we propose the following picture for Pt deposition on both vicinal surfaces of Au. The incoming Pt ad-atoms from the gas phase may condense on the Au surface initially without any appreciable site preference. However, at this point Pt ad-atoms or even nuclei formed by few atoms may diffuse on the terrace until they reach the lower part of the step edge. On both surfaces, the step edge acts as a barrier for diffusion and hence the growth of nuclei by the addition of incoming Pt proceeds by covering the terrace. In the specific case of Au(887), due to the reconstruction of the substrate two types of sites (fcc and hcp) emerge and so does an additional barrier for diffusion along the terrace. In agreement with the new surface structure after substrate reconstruction, Pt nanoislands with 1 to 3 ML height preferentially grow on fcc sites without filling up the hcp ones. Nevertheless, the addition of more Pt results in terrace coverage. On the contrary, since terraces on Au(332) do not reconstruct, ad-islands can freely grow along the terraces but confined within two contiguous step edges. On both surfaces, we find that as Pt coverage increases, nanoisland's height also increases, suggesting a 3D mode of growth at least at the highest coverage studied.

Finally, we found evidence (XPS results) of an exchange process between Pt and Au atoms on the topmost atomic layer or substrate/nanoisland interface that can be associated with surface alloying. The exchange mechanism has been identified by other authors for a similar system having a low density of

Table 1 BE obtained from fitting of XPS spectra in Fig. 5 for Pt/Au(332) and Pt/Au(887) samples

		Clean Au(332)	θ_{Pt} = 0.21 Pt/Au(332)	θ_{Pt} = 0.40 Pt/Au(332)	θ_{Pt} = 0.82 Pt/Au(332)	Clean Au(887)	θ_{Pt} = 0.16 Pt/Au(887)	θ_{Pt} = 0.29 Pt/Au(887)	θ_{Pt} = 0.59 Pt/Au(887)	θ_{Pt} = 1.48 Pt/Au(887)
Au $4f_{7/2}$/eV		83.7	83.8	83.7	83.7	84.0	84.0	84.0	84.0	84.0
	Comp. A	—	70.4	70.5	70.6	—	70.4	70.5	70.6	70.6
Pt $4f_{7/2}$/eV	Comp. B	—	71.4	71.5	71.4	—	71.4	71.5	71.5	71.4

defect by using chemical contrast in high resolution STM images. From all this, we conclude that the islands imaged with STM should not be entirely made of pure Pt.

It is worth mentioning that all the results presented so far are in excellent agreement with results reported for the Pt–Au system.[46–49] For instance, all these publications report the modifications of the catalytic properties of Pt by Au towards electrochemical reactions such as carbon monoxide, methanol and ethanol electrooxidation in the form of Pt/Au(*hkl*) surfaces or Pt–Au nanoparticles. In all cases, the poisoning of the surface by a stronger adsorption of CO in Pt–Au compared to pure Pt is reported as a consequence of the upward shift of the d-band centre of Pt due to electronic and/or geometrical effects induced by Au. In this sense, the core line shifts observed on XPS spectra of Pt $4f_{7/2}$ core line of component A for all samples, regardless of the crystallographic orientations of the underlying substrate, indicates that the insertion of Pt into gold (surface alloy formation) is mainly responsible for the d-band center shift (direction) observed in the case of Pt–Au nanoparticles and so, responsible for the stronger adsorption of CO at this surfaces compared to pure Pt. Interestingly, the magnitude of the core line shift seems to be independent on the crystallographic orientation of the underlying Au surface, suggesting that the electronic changes observed by XPS are independent of step density.

Moreover, recent publications[50,51] show that for Pt deposited on Au NPs, at low θ_{Pt}, the electrochemical oxidation of Pt atoms is inhibited. Our findings show that al low θ_{Pt} most of the Pt atoms form a Pt–Au surface alloy and, since Pt atoms would tend to be capped by Au atoms,[42] this could explain the inhibition of oxide formation at low Pt surface content on Pt/Au NPs.

The electrochemical oxygen reduction reaction (ORR) on these Pt/Au NPs was shown to occur by different mechanisms, at low and high Pt coverage.[50] The authors hypothesized that cluster formation at high coverage could be responsible for the changes in mechanism. We show that increasing θ_{Pt}, clusters from 1 ML up to 3 ML are formed.

Altogether, our findings agree well and explain the differences on the catalytic activity experimentally observed for Pt–Au surfaces when compared with pure Pt and also the differences observed for different Pt : Au surface ratios.

3.3 The effect of thermal annealing

In order to examine the effect of thermal annealing on the stability of Pt/Au(*hkl*) samples, selected samples were annealed under UHV up to 473 K for 10 min. STM images of the resulting Pt/Au(*hkl*) surfaces are shown in Fig. 6. As can be seen from the figure, in the case of the Pt/Au(332) surface, the structures originally present disappear leaving bright regions on the terraces (compared Fig. 3a and 6a). In the case of the sample with θ_{Pt} = 0.21 we observe the existence of bright region probably due to Pt insertion. However, when coverage increases to θ_{Pt} = 0.4, some features are still visible after annealing and, in some cases, the islands merged with neighbouring ones over a step edge thus occupying 2 terraces or more, instead of 1 (see circles in Fig. 6b).

On the other hand, the changes in the Pt/Au(887) surface seem to be a slightly different compared to Pt/Au(332). For instance,

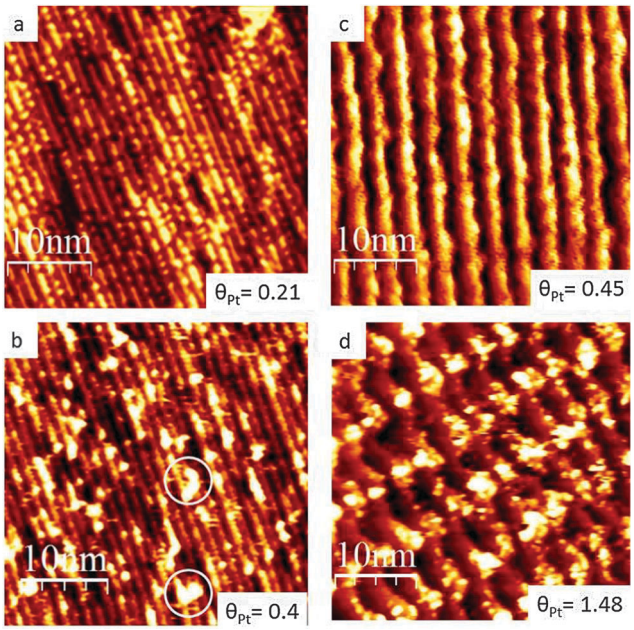

Fig. 6 STM images of samples annealed at 473 K. (a, b) Pt/Au(332) and (c, d) Pt/Au(887). Tunneling conditions: (a) V_{bias} = 1.25 V, I_t = 0.35 nA; (b) V_{bias} = 1.3 V, I_t = 0.41 nA; (c) V_{bias} = 1.25 V; I_t = 0.35 nA and (d) V_{bias} = 1.1 V; I_t = 0.17 nA.

the sample with θ_{Pt} = 0.45 ML show no features similar to the case of Pt/Au(332) with the same coverage. In the case of the (887) sample, Pt islands initially on fcc site are no longer visible after annealing, also due to Pt insertion as in the 0.21 ML Pt/Au(332) sample. Moreover, on both vicinal surfaces Pt insertion into Au seems to occur, during/after annealing, not only on step edges but also on terraces. However, when Pt coverage increases up to 1.48 ML, other effects of thermal annealing appear. As can be seen from Fig. 6d, the population of hcp site increases after thermal annealing and the number of hcp sites hosting Pt–Au nanoislands increases compared to the as-prepared sample (inset Fig. 3f). However, despite the existence of some remaining nanoislands on the surface, we believe that the same process of alloying that occurs at low coverage also occurs in this coverage range. The fact that some features identified as Pt are still visible can be related to the initial higher Pt concentration at the surface, *i.e.*, due to higher concentration of Pt, the time or even the temperature of the annealing was not enough to encapsulate all Pt deposited.

The insertion of Pt atoms into the Au matrix through the atom exchange mechanism has profound implications on the stability and reactivity of the modified surfaces. For instance, it is well established that Pt atom size is smaller compared to Au, as well as its lattice constant. In the case of incorporation into Au lattice, the resulting surface structure of the mixed Au–Pt layer will be affected by the presence of Pt, since due to the smaller size and lattice constant, the layer will be submitted to tensile stress, thus modifying the chemical and physical properties of the surface as a whole, a fact that has been experimentally observed for a collection of electrochemical reactions on Pt–Au nanoparticles.[50–52] Also, local modifications of surface atomic

distribution occur as a consequence of the insertion, thus modifying the geometry of the atomic ensemble needed for the reaction to proceed following a required reaction pathway, as discussed in detail in ref. 50 for the oxygen electrochemical reduction.

Considering what was already reported in the literature[38] surface strain does not seem to affect site preference (fcc *vs.* hcp sites) on reconstructed ($22 \times \sqrt{3}$) Au(111). However, the kinetics for surface diffusion is strongly affected by surface strain, due to changes in activation energy barriers. In this sense, it is clear from Fig. 6d that Pt features on the hcp-region of the reconstruction tend to locate at the lower part of the step edge rather than on the terrace where ''pure'' hcp sites reside, thus suggesting that the surface diffusion to the hcp site may occur through the step edges. The manual counting from Fig. 6d reveals that the majority of the mixed islands are BL (68%) or ML (20%) with some TL (12%) at fcc sites. On hcp region counting reveals that features have a ML height.

Furthermore, as discussed in the previous section, the alloying of Pt and Au is an endothermic process, *i.e.*, it corresponds to a thermally activated mechanism, as suggested by Gohda and Groß[43,53] using density functional theory (DFT) and other experimental papers published regarding Pt–Au bimetallic nanoparticles.[54,55] In this respect, these observations are in agreement with the results we are reporting for the annealed samples.

More insight can be gained about the effect of temperature on nanoisland's stability when photoelectron spectra are analysed. Table 2 contains some parameters resulting from the fitting of Pt $4f_{7/2}$ core line for all annealed samples such as BE of components and the ratio between component's areas. In all cases, as for the as-prepared samples, no changes in Au 4f photoemission core lines were observed upon annealing probably due to the strong contribution from bulk and hence, values are not shown in Table 2.

For both annealed Pt/Au(332) surfaces studied one can see that the same components ascribed to the Pt $4f_{7/2}$ core line before annealing are still present. Binding energy values obtained are slightly different from the values presented in Table 1 for the as-prepared samples having the same coverage and these differences can be ascribed to the precision of the fitting procedure. Moreover, if components ratio reported in Table 2 for the samples before and after annealing are compared, an increment on ratios value is perceived for both samples. This clearly confirms the idea of thermally-promoted alloying by Pt insertion suggested by the STM images in Fig. 6 and discussed before. As temperature rises the energy barrier for Pt diffusion into Au may be overcome and ad-atoms initially segregated on the surface are incorporated into the Au crystal lattice after annealing.

In the case of Pt/Au(887) samples the same trend is observed as in Pt/Au(332), *i.e.*, small changes in BE values for Pt $4f_{7/2}$ are observed compared to the as-grown ones. Moreover, when components ratio is analysed, for θ_{Pt} = 0.45 ML we see that the results obtained from XPS also agree with those from STM, *i.e.*, an increment of the ratio (increase in component A) due to further incorporation of Pt after annealing agrees with withdrawal of Pt features suggested in STM image of Fig. 6c. However, when the θ_{Pt} = 1.48 sample is analysed the result is a little bit different and somewhat contradictory if compared with the other samples. For instance, a decrease in the calculated ratio is obtained for the annealed sample. This would suggest that a segregation of Pt occurs upon annealing, a situation apparently incompatible with the thermal activated nature of the alloying process. However, if the STM images for the as-grown and annealed samples are compared (see inset Fig. 3f and 6d respectively), we see that a surface reorganization of the Pt nanostructures takes place upon annealing with a partial occupation of hcp sites, originally unoccupied. In this sense, by comparing the heights of Pt islands on fcc and hcp contiguous sites we may conclude that there is a migration of Pt from fcc to hcp that is only detected for the sample having the highest coverage of Pt. Thus, we believe that this particular behaviour may be responsible for the trend of component ratio observed in Table 2, where the variation of the calculated ratio may lie within the error associated with the area determination of the Pt 4f core line.

The results we showed in the previous pages are of great relevance from the fundamental point of view in the field of catalysis. For instance, we have demonstrated that from the point of view of reactivity of Pt nanoislands both electronic and geometric effects are equally important for the Pt–Au (vicinal) system. The fact that Pt alloys with the topmost layers of Au even at room temperature and especially after thermal annealing, implies that due to lattice mismatch the local properties of the Pt/Au(S)[$n(h_tk_tl_t) \times (h_sk_sl_s)$] surface should be different from the pure counterparts. The chemical shifts observed from XPS data for Pt $4f_{7/2}$ core photoemission lines also reflects the tensile stress experienced by Pt due to lattice expansion at the alloyed phase, since according to Gohda and Groß[43] a lateral expansion would cause an upward shift on Pt d-band center. On the other hand, we expect to see some changes on alloyed Au, although we were not able to detect any chemical shifts for the experimental conditions used. Finally, we show that platinum-modified gold vicinal surfaces may be used as model systems for the understanding of single crystal and also NPs surface catalytic properties.

Table 2 BE obtained from fitting of XPS spectra in Fig. 6 for annealed Pt/Au(332) and Pt/Au(887) samples. Fitted spectra are available in Fig. S3 of ESI

		θ_{Pt} = 0.21 Pt/Au(332)	θ_{Pt} = 0.40 Pt/Au(332)	θ_{Pt} = 0.45 Pt/Au(887)	θ_{Pt} = 1.48 Pt/Au(887)
Pt $4f_{7/2}$	BE Comp. A/eV	70.5	70.6	70.6	70.6
	BE Comp. B/eV	71.4	71.5	71.2	71.4
	(C_A/C_B) before annealing	3.4	1.8	3.1	2.5
	(C_A/C_B) after annealing	4.8	3.4	4.4	2.0

4. Conclusions

The electronic and morphological properties of Pt/Au(332) and Pt/Au(887) with different Pt coverage were studied using scanning tunneling microscopy (STM) and X-ray photoelectron spectroscopy (XPS). We were able to determine that deposition on both vicinal Au substrates occurs *via* an island formation mechanism with island's height being dependent of Pt content. Using STM we determined that a monolayer to bilayer transition occurs on both substrates, although the construction of a nanopattern occurs in the case of Au(887) due to the surface reconstruction of the substrate and in the case of Au(332) elongated nanostructures are formed along the step edges. In the case of Pt/Au(887) we suggest that Pt nanostructures having a height higher than 3 ML may be no longer stable, with the hcp-site being preferred as coverage increases (*e.g.* beyond 1.48 ML). XPS results reveal the existence of an alloyed Pt–Au phase and a segregated one. In the case of alloyed Pt, a negative shift in BE was observed at all samples, regardless of the crystallographic orientation of underlying Au. The extent of alloy formation was seen to change when samples are submitted to thermal treatment. For instance, the area ratio of the two different components at Pt $4f_{7/2}$ increases after annealing, suggesting the additional incorporation of Pt to the alloyed phase.

Also, the results presented in this paper show that on both vicinal surfaces studied platinum deposition occurs *via* island formation with nucleation at step edges. Moreover, the results agree well with the models proposed in the literature from theoretical calculations and help to explain the differences in the catalytic activity of reported chemical reactions of interest.

Acknowledgements

Authors thank Fundação de Amparo à Pesquisa do Estado de São Paulo (FAPESP-07/54829-5) and Conselho Nacional de Pesquisa (CNPq) for financial support. Specially thank to L. H. Lima for experimental assistance with STM measurements and Prof. G. Tremiliosi-Filho for lending the Au(332) crystal. MJP, SF and EAC thank FAPESP and CNPq for the fellowships granted (Procs. FAPESP 2011/12.566-3 and 2012/16860-6; Proc. CNPq 160172/2011-0).

References

1 J. Greeley, I. E. L. Stephens, A. S. Bondarenko, T. P. Johansson, H. A. Hansen, T. F. Jaramillo, J. Rossmeisl, I. Chorkendorff and J. K. Nørskov, *Nat. Chem.*, 2009, **1**, 552–556.
2 G. Wu, K. L. More, C. M. Johnston and P. Zelenay, *Science*, 2011, **332**, 443–447.
3 Y. H. Chu and Y. G. Shul, *Int. J. Hydrogen Energy*, 2010, **35**, 11261–11270.
4 A. Kowal, M. Li, M. Shao, K. Sasaki, M. B. Vukmirovic, J. Zhang, N. S. Marinkovic, P. Liu, A. I. Frenkel and R. R. Adzic, *Nat. Mater.*, 2009, **8**, 325–330.
5 C. W. Xu, Y. Z. Su, L. L. Tan, Z. L. Liu, J. H. Zhang, S. A. Chen and S. P. Jiang, *Electrochim. Acta*, 2009, **54**, 6322–6326.
6 F. Colmati, E. Antolini and E. R. Gonzalez, *J. Alloys Compd.*, 2008, **456**, 264–270.
7 E. Antolini, *J. Power Sources*, 2007, **170**, 1–12.
8 F. Colmati, E. Antolini and E. R. Gonzalez, *J. Power Sources*, 2006, **157**, 98–103.
9 V. R. Stamenkovic, B. S. Mun, K. J. J. Mayrhofer, P. N. Ross and N. M. Markovic, *J. Am. Chem. Soc.*, 2006, **128**, 8813–8819.
10 H.-J. Freund and G. Pacchioni, *Chem. Soc. Rev.*, 2008, **37**, 2224–2242.
11 Y. Kim, H. J. Kim, Y. S. Kim, S. M. Choi, M. H. Seo and W. B. Kim, *J. Phys. Chem. C*, 2012, **116**, 18093–18100.
12 Y. Kwon, Y. Birdja, I. Spanos, P. Rodriguez and M. T. M. Koper, *ACS Catal.*, 2012, **2**, 759–764.
13 R. G. Freitas and E. C. Pereira, *Electrochim. Acta*, 2010, **55**, 7622–7627.
14 F. Colmati, G. Tremiliosi, E. R. Gonzalez, A. Berna, E. Herrero and J. M. Feliu, *Phys. Chem. Chem. Phys.*, 2009, **11**, 9114–9123.
15 V. Repain, G. Baudot, H. Ellmer and S. Rousset, *Europhys. Lett.*, 2002, **58**, 730.
16 V. Repain, J. M. Berroir, S. Rousset and J. Lecoeur, *Europhys. Lett.*, 1999, **47**, 435.
17 Y. Nahas, V. Repain, C. Chacon, Y. Girard and S. Rousset, *Surf. Sci.*, 2010, **604**, 829–833.
18 S. Rohart, Y. Girard, Y. Nahas, V. Repain, G. Rodary, A. Tejeda and S. Rousset, *Surf. Sci.*, 2008, **602**, 28–36.
19 S. Rohart, G. Baudot, V. Repain, Y. Girard, S. Rousset, H. Bulou, C. Goyhenex and L. Proville, *Surf. Sci.*, 2004, **559**, 47–62.
20 G. Axel, *J. Phys.: Condens. Matter*, 2009, **21**, 084205.
21 J. Rodriguez, *Surf. Sci. Rep.*, 1996, **24**, 223–287.
22 M. Eyrich, T. Diemant, H. Hartmann, J. Bansmann and R. J. Behm, *J. Phys. Chem. C*, 2012, **116**, 11154–11165.
23 M. Bowker, *Chem. Vap. Deposition*, 1995, **1**, 90.
24 J. B. Xu, T. S. Zhao, W. W. Yang and S. Y. Shen, *Int. J. Hydrogen Energy*, 2010, **35**, 8699–8706.
25 J. Wang, G. Yin, G. Wang, Z. Wang and Y. Gao, *Electrochem. Commun.*, 2008, **10**, 831–834.
26 I. Horcas, R. Fernandez, J. M. Gomez-Rodriguez, J. Colchero, J. Gomez-Herrero and A. M. Baro, *Rev. Sci. Instrum.*, 2007, **78**, 013705–013708.
27 S. Doniach and M. Sunjic, *J. Phys. C: Solid State Phys.*, 1970, **3**, 285.
28 S. E. Hörnström, L. Johansson, A. Flodström, R. Nyholm and J. Schmidt-May, *Surf. Sci.*, 1985, **160**, 561–570.
29 N. J. Shevchik, *Phys. Rev. Lett.*, 1974, **33**, 1336.
30 C. J. Powell, *J. Electron Spectrosc. Relat. Phenom.*, 2012, **185**, 1–3.
31 S. Rousset, V. Repain, G. Baudot, Y. Garreau and J. Lecoeur, *J. Phys.: Condens. Matter*, 2003, **15**, S3363.
32 G. Prévot, Y. Girard, V. Repain, S. Rousset, A. Coati, Y. Garreau, J. Paul, N. Mammen and S. Narasimhan, *Phys. Rev. B: Condens. Matter Mater. Phys.*, 2010, **81**, 075415.
33 V. Repain, S. Rohart, Y. Girard, A. Tejeda and S. Rousset, *J. Phys.: Condens. Matter*, 2006, **18**, S17.

34 V. Repain, G. Baudot, H. Ellmer and S. Rousset, *Mater. Sci. Eng., B*, 2002, **96**, 178–187.
35 V. Repain, J. M. Berroir, S. Rousset and J. Lecoeur, *Surf. Sci.*, 2000, **447**, L152–L156.
36 P. Campiglio, V. Repain, C. Chacon, O. Fruchart, J. Lagoute, Y. Girard and S. Rousset, *Surf. Sci.*, 2011, **605**, 1165–1169.
37 M. J. Prieto, E. A. Carbonio, R. Landers and A. de Siervo, *Surf. Sci.*, 2013, **617**, 87–93.
38 G. Antczak and G. Ehrlich, *Surface Diffusion: Metals, Metal Atoms, and Clusters*, Cambridge Univesrity Press, New York, 2010.
39 S. Y. Kim, I.-H. Lee and S. Jun, *Phys. Rev. B: Condens. Matter Mater. Phys.*, 2007, **76**, 245407.
40 Y. B. Liu, D. Y. Sun and X. G. Gong, *Surf. Sci.*, 2002, **498**, 337–342.
41 G. Prévot, L. Barbier and P. Steadman, *Surf. Sci.*, 2010, **604**, 1265–1272.
42 M. Ø. Pedersen, S. Helveg, A. Ruban, I. Stensgaard, E. Lægsgaard, J. K. Nørskov and F. Besenbacher, *Surf. Sci.*, 1999, **426**, 395–409.
43 Y. Gohda and A. Groß, *Surf. Sci.*, 2007, **601**, 3702–3706.
44 E. Pastor, J. L. Rodriguez and T. Iwasita, *Electrochem. Commun.*, 2002, **4**, 959–962.
45 J. K. Keister, J. E. Rowe, J. J. Kolodziej and T. E. Madey, *J. Vac. Sci. Tech. B*, 2000, **18**, 2174–2178, DOI: 10.1116/1.1305872.
46 R. Martin, P. Gardner and A. M. Bradshaw, *Surf. Sci.*, 1995, **342**, 69–84.
47 S. R. Bare, P. Hofmann and D. A. King, *Surf. Sci.*, 1984, **144**, 347–369.
48 S. Yamagishi, T. Fujimoto, Y. Inada and H. Orita, *J. Phys. Chem. B*, 2005, **109**, 8899–8908.
49 S. Watanabe, J. Inukai and M. Ito, *Surf. Sci.*, 1993, **293**, 1–9.
50 A. Sarkar, J. B. Kerr and E. J. Cairns, *ChemPhysChem*, 2013, **14**, 2132–2142.
51 B. Du, O. Zaluzhna and Y. J. Tong, *Phys. Chem. Chem. Phys.*, 2011, **13**, 11568–11574.
52 B. J. Auten, H. Lang and B. D. Chandler, *Appl. Catal., B*, 2008, **81**, 225–235.
53 Y. Gohda and A. Groß, *J. Electroanal. Chem.*, 2007, **607**, 47–53.
54 T. Kobiela, M. Moors, W. Linhart, I. Cebula, A. Krupski, C. Becker and K. Wandelt, *Thin Solid Films*, 2010, **518**, 3650–3657.
55 V. Petkov, B. N. Wanjala, R. Loukrakpam, J. Luo, L. Yang, C.-J. Zhong and S. Shastri, *Nano Lett.*, 2012, **12**, 4289–4299.